USGS
science for a changing world

Numerical Simulation of Waves and Sediment Transport Along a Transgressive Barrier Island

Chapter H of
Sand Resources, Regional Geology, and Coastal Processes of the Chandeleur Islands Coastal System: an Evaluation of the Breton National Wildlife Refuge

Scientific Investigations Report 2009–5252

U.S. Department of the Interior
U.S. Geological Survey

Numerical Simulation of Waves and Sediment Transport Along a Transgressive Barrier Island

By Ioannis Y. Georgiou and Jennifer Schindler

Chapter H of

Sand Resources, Regional Geology, and Coastal Processes of the Chandeleur Islands Coastal System: an Evaluation of the Breton National Wildlife Refuge

Edited by Dawn Lavoie

In cooperation with the U.S. Fish and Wildlife Service

Scientific Investigations Report 2009–5252

U.S. Department of the Interior
U.S. Geological Survey

U.S. Department of the Interior
KEN SALAZAR, Secretary

U.S. Geological Survey
Marcia K. McNutt, Director

U.S. Geological Survey, Reston, Virginia: 2009

This and other USGS information products are available at http://store.usgs.gov/
U.S. Geological Survey
Box 25286, Denver Federal Center
Denver, CO 80225

To learn about the USGS and its information products visit http://www.usgs.gov/
1-888-ASK-USGS

Suggested citation:
Georgiou, I.Y., and Schindler, J., 2009, Chapter H. Numerical simulation of waves and sediment transport along a transgressive barrier island, *in* Lavoie, D., ed., Sand resources, regional geology, and coastal processes of the Chandeleur Islands coastal system—an evaluation of the Breton National Wildlife Refuge: U.S. Geological Survey Scientific Investigations Report 2009–5252, p. 143–168.

Chapter H. Numerical Simulation of Waves and Sediment Transport Along a Transgressive Barrier Island

By Ioannis Y. Georgiou[1] and Jennifer Schindler[1]

Abstract

Louisiana barrier islands, especially the chain surrounding the southeast region that encompasses Chandeleur and Breton Sounds, are undergoing rapid loss of land and extreme landward migration rates because of transgressive submergence and the landfall of several major hurricanes in the last decade. Migration rates and overall impacts to these barrier islands are poorly understood since they do not respond in a traditional way, such as barrier island rollover. To quantify the response to low-intensity, intermediate, and extreme events, as well as their recovery, a suite of computational tools were employed to help characterize the remote and local forcing on the barrier islands. The results from this study were compared against field observations (where available), observations and overall trends from sea floor change, and historical shoreline change trends. It was concluded that the barrier islands are undergoing high rates of transport in the northward direction during intermediate and high-intensity storms, that vast areas of the lower shoreface are activated and are undergoing erosion during these events, and that there is little or no fair weather mechanism to rework material into the littoral system. As a result, there is a net loss from the system.

Introduction and Background

The Chandeleur Islands (fig. 1), the largest barrier island arc in southeast Louisiana, formed from the abandonment of the St. Bernard Delta Complex approximately 2,000 years before present (BP) (Penland and others, 1988; Suter and others, 1988). While substantial research has historically been conducted along this barrier island chain, it was primarily focused on geomorphic response, evolution, historical shoreline change, and area change based on aerial and satellite imagery and framework geology. The literature regarding quantification of short-term physical processes, the historical physical processes, and the physics that drive the evolution of the barrier islands—such as waves, hydrodynamics, and resulting sediment transport—is rather limited (Georgiou and others, 2005; Ellis and Stone, 2006). These processes (which have not been well studied, measured, or understood) take place over multiple spatial and temporal scales and are extremely difficult to measure, quantify, and accurately describe. These complexities present challenges in attempts to numerically parameterize and use in forecasting relations, and in the absence of measurements, predictions can be rather unreliable when based upon assumptions or inferences that are not directly measured. Furthermore, measurements and attempts to capture all temporal and spatial scales are nearly impossible. The study of the Chandeleur Islands herein employed a reanalysis of the currently available historical wind and wave climate that drove the response and recovery of the barrier islands, the quantification of historical longshore sediment transport trends resulting from both fair weather and storms, and a first-order attempt to simulate event-driven response to storm waves and implications for sediment transport.

For this study, we employed simple wave forecasting by using a long-term dataset of offshore winds, applying simple transformation to breaking to get predictions of longshore sediment transport by using the Coastal Engineering Research Center (CERC; 1977) equation. These predictions were subsequently used to generate transport gradients to determine erosion and deposition areas along the Chandeleur Islands arc to help validate the landward migration of the barrier islands. Offshore deepwater wave buoys were also used to generate storm waves of different return periods (1, 10, and 100 years) by using the peak over threshold (POT) method and were fitted to a Gumbel distribution. These storm waves were then propagated across the continental shelf, onto the barrier islands, inland into sounds and interior wetlands, to identify a mechanism for shoreface erosion. Propagation was achieved with the Simulation of WAves Nearshore (SWAN) numerical model (Holthuijsen and others, 1993). Finally, and since the shoreface is primarily composed of muddy substrate, tidal and storm-induced circulation in the vicinity of the Chandeleur Islands was conducted to identify potential pathways for shoreface material eroded during these events.

[1] University of New Orleans, Pontchartrain Institute for Environmental Sciences, New Orleans, La.

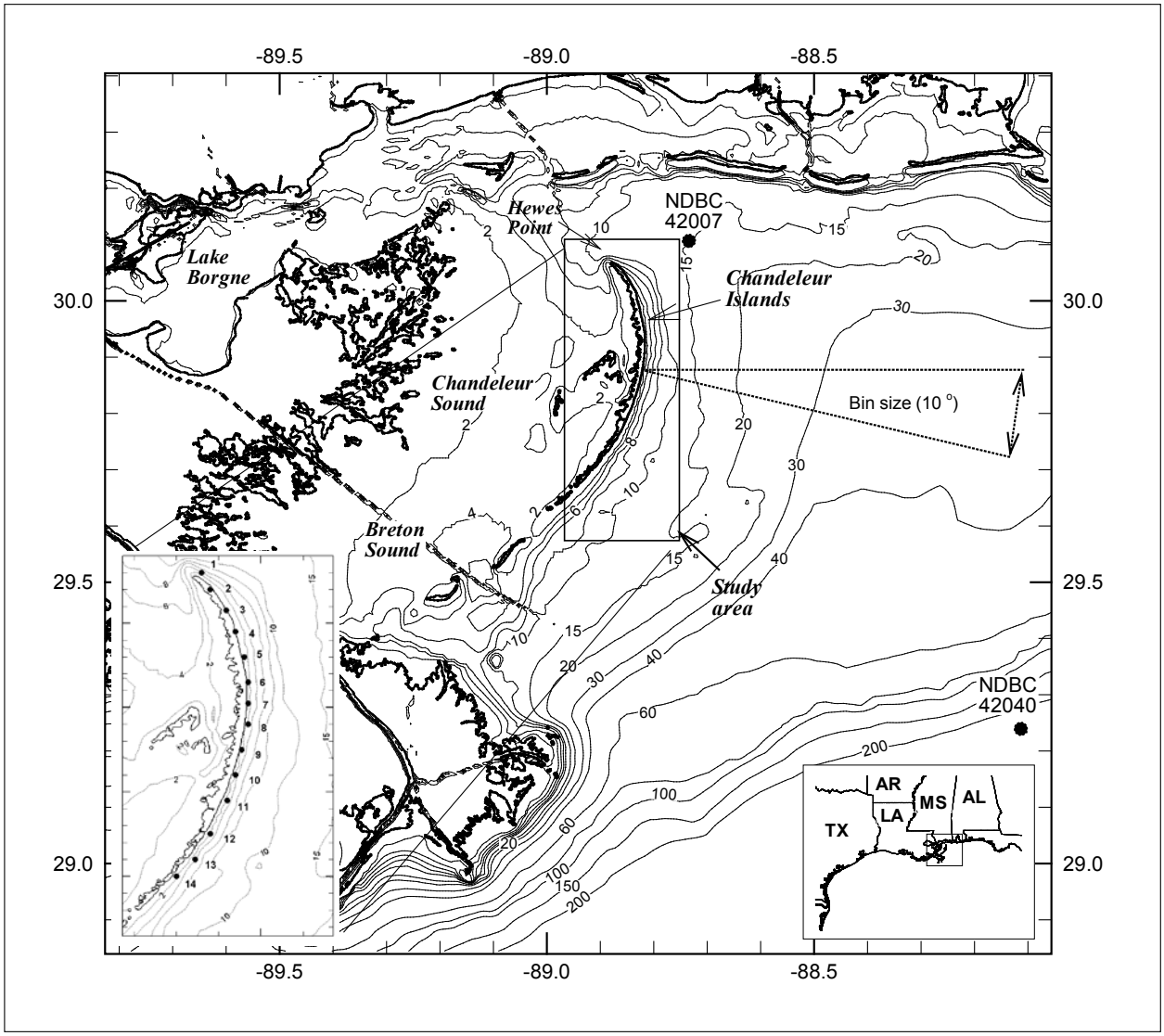

Figure 1. Regional map of the study area in the vicinity of the Chandeleur Islands, La., showing the locations of the 14 points used in the wave forecasting and alongshore sediment transport calculations (left inset map), the locations of two National Data Buoy Center (NDBC) buoys (solid circles), Hewes Point, and regional bathymetry.

Methods and Materials

Wind and Wave Climate Analysis

The present-day wave and wind climate in the vicinity of the Chandeleur Islands is unknown. To characterize the wave energy and regional wind along the barrier islands, the nearest wave buoy from the the National Oceanic and Atmospheric Administration (NOAA) National Data Buoy Center (NDBC) was used. This wave buoy—a 3-m discus buoy reporting hourly observations with historical data since 1985—is NDBC station 42007, positioned 22 nautical miles (nmi) south-southwest of Biloxi, Miss., located at 30.09 degress North 88.77 degrees West (fig. 1). NDBC data streams were imported into wind rose analysis software (WRPLOT View, Lakes Environmental Software, Waterloo, Ontario, Canada) and were plotted and analyzed. We used a 10-degree directional bin for both wind and wave classification, while

seven magnitude bins were used to capture the range within each record. Missing file indicators were defined to generate accurate wind rose plots and wind probabilities, excluding missing data records from frequency plots and counts. Frequency distribution, frequency count, and wind rose plots for each year (1985–2006) were produced. Wind rose plots divide wind data into 36 directional bins and 7 windspeed classes. The records were subsequently split into three categories for further analysis and to develop seasonal trends. These three categories are annual, period 1 (which corresponds to the cold front season, from November 1 through March 30), and period 2 (which corresponds to the remaining part of the year, from April 1 through October 30). This classification enabled a comparison of the wind and wave climate between the hurricane season and the cold front season. For the annual analysis, 4 of the years during the period of 1985 through 2006 that had the minimum number of missing records were used, namely years 1989, 1994, 1999, and 2006. The missing records for these years were typically 5–15 percent of the total annual record.

One-Dimensional Wave Modeling and Longshore Sediment Transport

A set of 14 points equally spaced across the barrier island chain were selected, with the first point located near Hewes Point, La., on the north end of the barrier island chain at 30.05 degrees North and the last point located south near 29.70 degrees North (fig. 1, inset). The same records used for the wind and offshore wave climate analysis were also used to create input files to drive a one-dimensional wave modeling and resulting longshore sediment transport model. Fetch and a depth profile were extracted along each radial line shown in figure 2 and were used for wave generation, propagation, and transformation. Wave generation along the radial lines (fig. 2) was computed with windspeed and direction observed at station 42007. Waves were assumed to be of zero height at the end of the radial lines (fig. 2), seas were assumed to be fully developed, and waves were assumed to be duration limited, except for waves approaching from

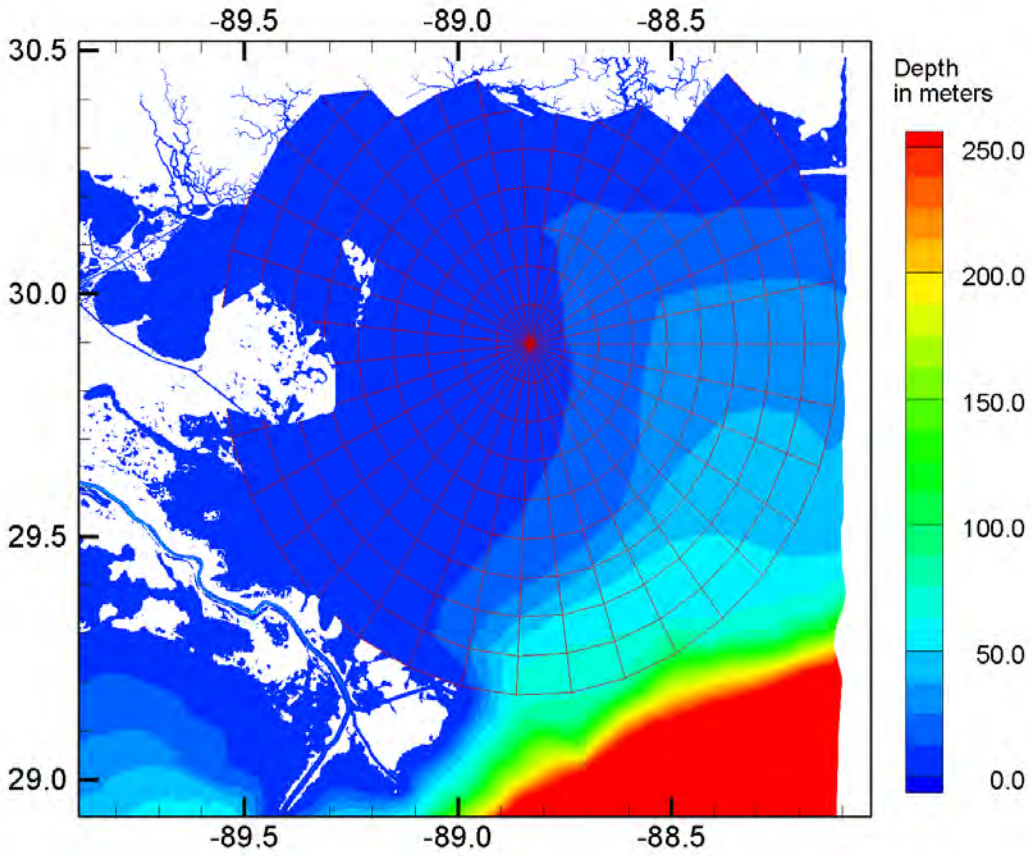

Figure 2. Circular pattern showing the directional bin size and typical extent for the one-dimensional wave generation, propagation, and longshore sediment transport calculations for the Chandeleur Islands, La. Each of the 14 equally spaced locations along the barrier island chain has a similar pattern.

the northeast, where fetch-limited waves may be generated. Waves were transformed from deep to shallow water by incorporating effects due to refraction, shoaling, and breaking. Refraction coefficients (K_r), shoaling coefficients (K_s), and breaker indexes (K_b) were computed for each wave that was generated (every hour) by using the power transmission equation, defined as

$$\frac{H_1}{H_0} = K_s K_r \qquad (1)$$

where H_1 is the shallow water wave height and H_0 is the deep water wave height. The refraction coefficient (K_r) was defined by

$$K_r = \sqrt{\frac{\cos(\alpha_0)}{\cos(\alpha_1)}} \qquad (2)$$

where α_0 is the deep water wave angle and α_1 is the shallow water wave angle. The shoaling coefficient (K_s) was defined by

$$K_s = \sqrt{\frac{1}{2n_1 \tanh\left(\frac{2\pi d}{L_1}\right)}} \qquad (3)$$

where L_1 is the shallow water wave length and n_1 is the fraction of wave energy being transmitted = $\frac{C_{gb}}{C}$. The group celerity at the breaker line, C_{gb}, is given by

$$C_{gb} = \sqrt{gd_b} = \sqrt{g\frac{H_b}{K_b}} \qquad (4)$$

where $K_b = \left(\frac{H_b}{d_b}\right)$ represents the breaker index, taken as $K_b = 0.78$ for a flat beach. Similarly, the shallow water wave celerity (C) is computed as $C = \sqrt{gd}$.

The wave angle was recorded at breaking and was used in reference to the coastline azimuth to produce the wave incident angle for the longshore sediment transport computation. The longshore sediment transport was then computed on the basis of the frequency of each wave occurring from a specific direction and magnitude bin for a record of 1 year as a percentage by using hourly data records. The CERC longshore transport equation (Coastal Engineering Research Center, 1977) was used to compute the potential transport of quartz sand with a sediment density of 2,650 kg/m^3. The cumulative southward and northward transport was calculated at each of the 14 locations, and the difference of the transport was recorded as the net transport for each location. For all wind records, windspeeds were corrected by using the 0.11 power law (Peterka and Shahid, 1998). Since the 42007 buoy anemometer is at 5 m, a correction was applied as follows:

$$(V_{\text{corrected}}) = (V_{\text{actual}}) * (10.0/Z_a)^{0.11} \qquad (5)$$

where Z_a is the station's anemometer height in meters, $V_{\text{corrected}}$ is the windspeed corrected for an anemometer height of 10 m, and V_{actual} is the original windspeed measured at a height of Z_a.

Two-Dimensional Wave Modeling and Transport

SWAN Modeling

The Simulation of WAves Nearshore (SWAN) (Holthuijsen and others, 1993) simulation program was used to propagate wave energy on the barrier island chain during storms. A computational domain with 600-m resolution covering the entire area of the Breton and Chandeleur Sounds, east to the outer continental shelf (fig. 3), was also used to propagate storm wave energy. This domain was nested twice, once covering the Chandeleur Islands with a 250-m resolution and once more near Hewes Point with a 50-m resolution. The eastern boundary for the large domain extended to the location of the NDBC buoy 42040. Observations from this buoy (which was operating during both Hurricane Ivan and Hurricane Katrina within hours of the storms passing from

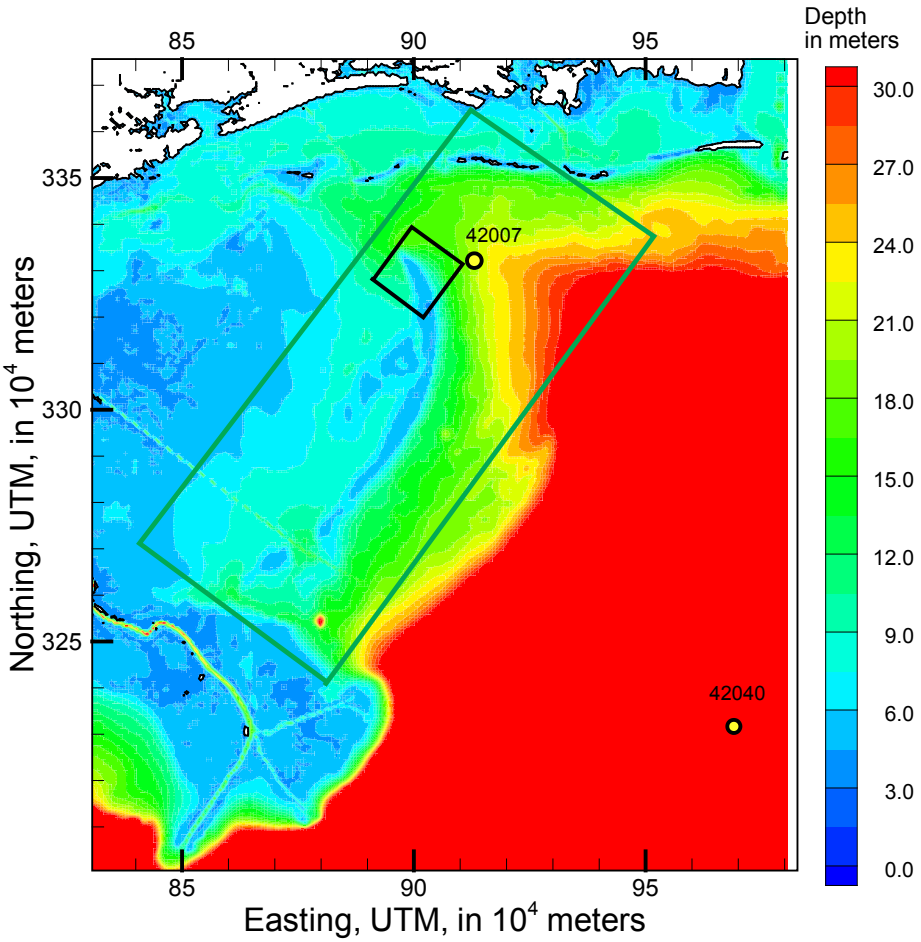

Figure 3. Overview of computational domains and boundaries of the numerical model Simulating WAves Nearshore (SWAN; Holthuijsen and others, 1993) for the Chandeleur Islands, La. Extent of the bathymetry file covers the large grid with 600-m resolution, the green grid covers the first nest grid with 250-m resolution, and the small black grid covers the second nest grid with 50-m resolution. The National Data Buoy Center (NDBC) buoy locations used for boundary condition and validation are also given in circles with their respective numbers/names. For clarity, contours greater than 30 m are not shown. UTM, Universal Transverse Mercator.

the area) were used to generate the storm wave characteristics at the boundary of the SWAN model. Since extreme statistics cannot be used because of the short record available at the station, the peak over threshold (POT) method was used. The data were fitted into a Gumbel distribution to extrapolate the extreme storm wave values for the 1-year, the 10-year, and the 100-year storm. (We emphasize that the data only covered a period of 10 years; hence, the extrapolation to a 100-year storm is a combination of statistics using the Gumbel distribution, as well as methodology used in the Interagency Performance Evaluation Taskforce [U.S. Army Corps of Engineers, 2006] during Hurricane Katrina statistics on return period.) Model-derived storm surge levels resulting from tropical activity and extreme events (Resio and Westerink, 2008) indicate that water levels during Katrina reached 4 m at the peak of the storm in the vicinity of the study area. Tidal range in the vicinity of the barrier islands is small (about 0.8 m). By using this information and expert judgment regarding storm track, forward speed, and other storm parameters, storm surge levels to accompany the storm waves for the 100-year, 10-year, and 1-year events were estimated at 4 m, 3 m, and 1.5 m above mean sea level.

Tidal and Storm-Induced Circulation

Tidal circulation in the vicinity of the Chandeleur Islands is not well known. There exist very little data to describe tidal

range and tidal velocities. To help meet this need, an existing validated numerical model (McCorquodale and others, 2008), based on the Finite Volume Coastal Ocean Model (FVCOM) originally developed by Chen and others (2003), was used to extract regional and local tidal currents, tidal range, and transport trends resulting from fair weather tidal motion. For circulation and velocity distribution and water level time histories during storms, the Advanced Circulation (ADCIRC) model was used (Resio and Westerink, 2008). Results and analysis for simulations from existing and previous U.S. Army Corps of Engineers efforts were requested, obtained, and analyzed accordingly (U.S. Army Corps of Engineers, 2006; Smith and others, 2007; Sleath and others, 2009).

Results

Wind and Wave Climate Analysis

Wind climate analysis generally indicated that while the annual wind and wave distribution at the NDBC buoy 42007 was relatively evenly distributed there were changes in the directional distribution and dominance with seasons. Period 1 (fig. 4*A*) had a dominant weighted direction from the southeast and northwest, confirming the typical response of cold fronts in which winds are generally from the southeast prior to the cold front and switch to the northwest once the front has passed through. Period 2 (fig. 4*B*) did not have a clear dominant weighted direction but generally showed higher magnitude winds from the northeast, southeast, and southwest. When combined, the annual resultant wind vector was from the east-southeast. Significant wave heights in the vicinity of the northern portion of the barrier islands appeared to be fairly similar for all years (fig. 4*C*, right), with a peak of 0.45 m (long-term hourly average for 25 years) and a skewed population. The tail of the population showed that significant wave heights in excess of 1 m occur approximately 4 percent of the year, while 2-m waves are rather rare, with return periods of less than 1 percent. Seasonal wind climate analysis showed similar results (figs. 4*A* and 4*B*, left). The peak significant wave heights for the cold front season had a slightly lower frequency (about 11 percent) and lower peaks in the wave heights (approximately 0.4 m; fig. 4*A*, right). During the hurricane season, however, wave heights of similar magnitude (about 0.5 m) appeared to have a frequency of nearly 17 percent (fig. 4*B*, right).

One-Dimensional Longshore Sediment Transport

There is a net southern transport for locations south of the central segment of the barrier islands and a net northward transport on the northern portion of the barrier islands (fig. 5). Since the offshore NDBC buoys do not record wave direction, the wind distribution (shown in figs. 4*A*–4*C*) is often used to define wave direction, which was the case for all simulations herein for the one-dimensional model. Furthermore, period 1 covers the entire cold front season, during which abrupt changes in speed and direction are expected fairly often (frequency of 7–10 days; see fig. 4*A*, which shows that a significant amount of the wind distribution is from the northwest). These winds will produce completely different waves nearshore of the barrier islands and subsequently produce different transport trends.

When all of the records representing 25 years of wind at this station are used to generate and propagate waves onshore, longshore sediment transport trends can be computed. For each of the 14 locations in figure 5, waves were propagated to breaking, and depending on the breaking angle and local breaker height and assuming a sandy bottom, potential longshore sediment transport was computed by using the CERC equation (Coastal Engineering Research Center, 1977) and Komar (1998). The underlying assumption was that the waves generated would have similar direction to that of the observed wind in deep water. Comparisons of observed wave heights to those predicted by the Waves Information Studies (Hubertz, 1989) project showed that there are some discrepancies, but overall the assumption was assumed satisfactory. Each set of wave generation, propagation, and transformation was executed 8,760 times a year for 4 years and for 14 locations (total of 490,560 simulations). An additional 50,000 simulations were conducted to assess sensitivity on (1) atmospheric stability (gradient between air and sea surface temperature), (2) windspeed, (3) fetch, and (4) depth. The net transport was then computed as the net difference between north and south transport at each of the 14 locations. Figure 5 includes an uncertainty band for each location shown as “error bars”; this band was estimated on the basis of the cumulative effects of sensitivity analysis performed, which included variations in windspeed, atmospheric stability (the air-water temperature at the buoy was used here to set the stability parameter), fetch, and depth. The sensitivity analysis was performed to provide a quantitative measure of the resulting changes in transport because the methodology incorporates several parameterizations. The differencing of the net transport at each location was furthermore differenced along the barrier island chain to produce a transport gradient (sediment volume per unit time, per unit length of the barrier island chain) (table 1).

We found that the long-term transport trend is characterized by a bidirectional system (fig. 5), which is similar to observations by Georgiou and others (2005) and Ellis and Stone (2006). While differences exist in the determination of the nodal point between the literature and this study, the nodal point predictions are only 3–5 km apart. While wind and wave conditions are similar, local bathymetry contours, changes in barrier island configuration, and location

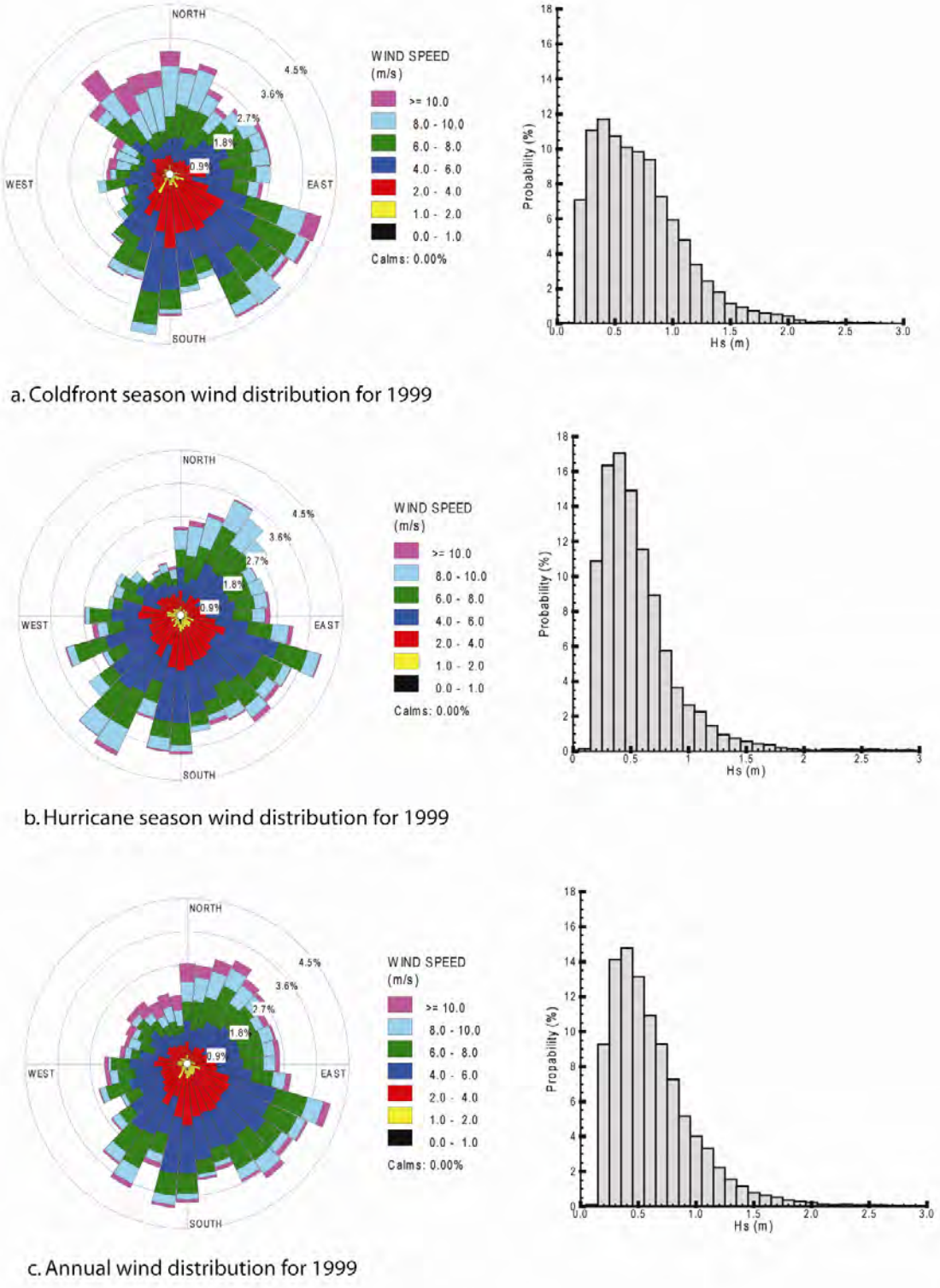

Figure 4. Seasonal wind distribution and significant wave height probability at National Data Buoy Center (NDBC) buoy 42007 in the vicinity of the Chandeleur Islands, La. *A*, Annual wind distribution for 1999 and significant wave height probability. *B*, Cold front season (period 1) wind distribution for 1999 and significant wave height probability. *C*, Hurricane season (period 2) wind distribution for 1999 and significant wave height probability.

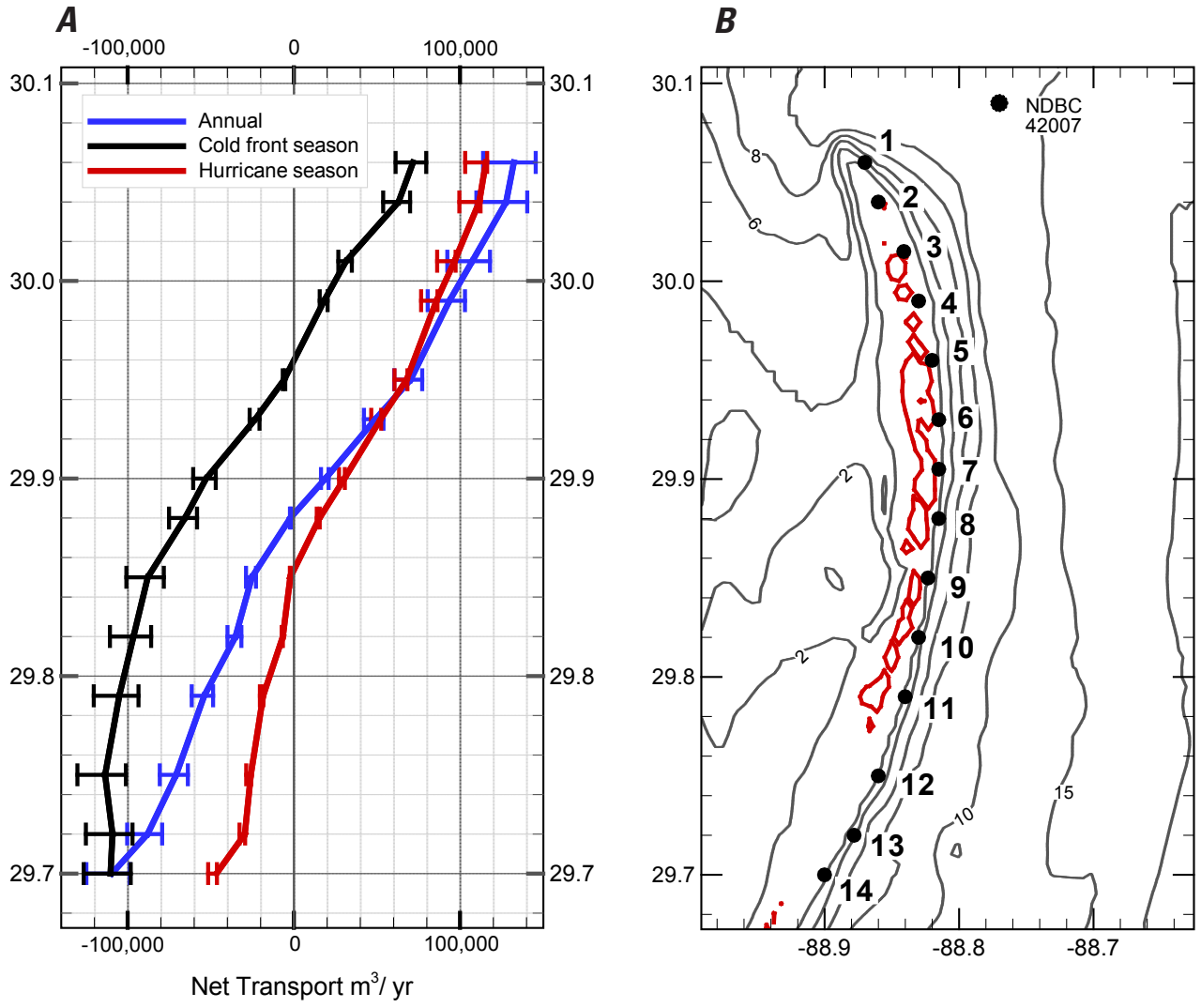

Figure 5. *A*, Seasonal changes in the potential net longshore transport rates across the northern Chandeleur Islands arc as a result of long-term annual forcing (blue line), hurricane season forcing (red line), and cold front season forcing (black line). *B*, The post-Hurricane Katrina subaerial island extent in relation to the location of the 14 points used in the wave predictions.

would cause predictions to be different. Transport magnitudes were also similar to the literature (Ellis and Stone, 2006) with transport rates in the northern portion of the barrier islands varying from 60,000 to 130,000 m^3/yr and approximately 50,000 to 110,000 m^3/yr for the southern part of the barrier islands. Transport gradients range from 0.3 to 6 m^3/m/yr in the southern part of the barrier islands, while the northern part can undergo gradients of 6 m^3/m/yr. Sensitivity analysis and seasonal forcing indicated that the transport rates and gradients vary seasonally and can undergo variations from 0.5 to 2 times the long-term average during seasons. During the summer season, for example, transport to the south can decrease to 50,000 m^3/yr. These variations in transport rates are responsible for the oscillations to the nodal point.

Two-Dimensional Wave Modeling

SWAN Wave Modeling Setup and Results—Storm Weather Simulations

Statistics to characterize storm waves in the vicinity of the northern Gulf of Mexico were completed by using the

Table 1. Summary of seasonal changes in the net longshore sediment transport rates and transport gradients.

[Note the resulting gradients produced by differencing the transport rates. Positive gradients indicate deposition, while negative gradient indicates erosion. m, meters; yr, year]

Point	Latitude	Segment distance (m)	Annual (long-term)		Cold front season		Hurricane season	
			Net transport (m^3/yr)	Gradient (m^3/m/yr)+	Net transport (m^3/yr)	Gradient, (m^3/m/yr)+	Net transport (m^3/yr)	Gradient, (m^3/m/yr)+
1	30.06		132,480		71,831		115,600	
2	30.04	2422	127,814	-1.9	63,086	-3.6	111,665	-1.6
3	30.01	3470	107,443	-5.9	31,494	-9.1	96,764	-4.3
4	29.99	2940	93,765	-4.7	18,359	-4.5	85,930	-3.7
5	29.95	4445	70,336	-5.3	-5,742	-5.4	67,955	-4.0
6	29.93	2222	49,147	-9.5	-23,113	-7.8	52,316	-7.0
7	29.90	3470	19,104	-8.7	-52,712	-8.5	30,561	-6.3
8	29.88	2422	-1,972	-8.7	-65,375	-5.2	15,589	-6.2
9	29.85	3334	-25,174	-7.0	-87,776	-6.7	-2,084	-5.3
10	29.82	3470	-34,932	-2.8	-96,383	-2.5	-6,530	-1.3
11	29.79	3334	-53,830	-5.7	-104,899	-2.6	-18,351	-3.5
12	29.75	4445	-70,690	-3.8	-113,475	-1.9	-25,761	-1.7
13	29.72	3470	-87,886	-5.0	-109,004	1.3	-29,412	-1.1
14	29.70	3650	-109,423	-5.9	-110,180	-0.3	-46,471	-4.7
		Average	15,442	-5.7	-41,706	-4.4	31,984	-3.9
		Standard deviation	82,305	2.3	67,158	3.2	56,065	2.0

* Positive transport is north; negative transport is south.

** Positive gradient indicates deposition; negative indicates erosion.

+ Transport gradients correspond to a location in the middle of points.

NDBC buoy 42040. By using the peak over threshold (POT) method and a fitted Gumbel distribution, the storm waves for the 100-year, 10-year, and 1-year storms were generated (table 1).

Initial and boundary conditions (table 2) were then applied to the boundary of the large computational domain. The frequency range was set to 0.025–0.8 Hz and $\Delta f = 0.1f$. The large grid was mainly intended to propagate wave energy to the nested grids. The SWAN model will ultimately use an f^{-5} diagnostic tail for wave input above the cutoff frequency if needed. The directional space was discretized with 36 bins of 10 degrees over the full directional circle. Default convergence criteria were imposed. For situations in which large gradients in currents and bottom profile are expected (which is not the case here), a stricter criterion can be used. None of the simulations reached an iteration count of 15. The following physical settings were also applied (these are default in SWAN, except the whitecapping formulation of van der Westhuysen [van der Westhuysen and others, 2007]). Quadruplets were automatically accounted for when wind was applied. Default wave breaking was used. Friction was accounted for by a default Joint North Sea Wave Project (JONSWAP) criterion for general wind sea waves (for swell waves an alternative constant should be used).

A boundary condition was applied at the southern and eastern sides of the grid by using a JONSWAP spectrum, described by the H_{m0}, T_p, peak enhancement factor gamma (default 3.3). Direction spreading was assumed to be described with $\cos^2(\theta)$. For wave and wind directions 90 degrees to 225 degrees, a constant boundary condition was applied on both boundaries. This condition was sufficient to describe the wave condition at the boundary, as the model quickly adapted to local driving conditions within a few hundred meters inside the model domain boundary. For waves with incident

Table 2. Statistical estimate of return periods for wind, waves, and water level based on Gumbel distribution for different storm conditions applied as boundary conditions at the seaward open boundary in the numerical model Simulating WAves Nearshore (SWAN; Holthuijsen and others, 1993) for the Chandeleur Islands, La.

[m, meters; s, seconds; NAVD 88, North American Vertical Datum of 1988]

	100-year storm	10-year storm	1-year storm
H_{mo} (m)	20	14	6.5
T_p (s)	17	13.5	9
Water level elevation (m) in NAVD 88	4	3	1.5
Wind speed (m/s)	42	28	19

Table 3. Boundary conditions applied for the 45-degree calculation.

[m, meters; s, seconds]

		1-year storm	10-year storm	100-year storm
Boundary condition 1	H_{mo} (m)	3.2	2.5	2
	T_p (s)	7	6	5
Boundary condition 2	H_{mo} (m)	6.5	4.5	3
	T_p (s)	9.5	8	6.5

Table 4. Comparisons between predictions made by using the Simulating WAves Nearshore (SWAN) numerical model and observations during a Hurricane Katrina hindcast.

[m, meters; s, seconds; NDBC, National Data Buoy Center]

	Predicted with SWAN	Observed at NDBC buoy 42007	Difference (predicted - observed) +/-%
H_{m0} (m)	5.38	5.64	-5
T_{m01} (s)	8.44	8.1	4
T_p (s)	13.87	14.3	-3

angles of 45 degrees, it would be unrealistic to use the wave conditions shown in table 2 for the entire eastern boundary because of the proximity of land near the northern portion of the eastern boundary; hence, a simple Bretschneider's formula was used to account for finite wave growth occurring beyond the boundary. Additionally, an increasing wave spectrum was assumed starting at $H_{m0} = 1$ and $T_p = 4$ to values of H_{m0} and T_p (table 3) calculated by using Bretschneider's formula for the northernmost part of the eastern boundary and interpolated to deepwater conditions to the southeast corner of the boundary.

The model was validated by using a Hurricane Katrina hindcast stationary wave simulation using boundary conditions produced by Smith (2007). The simulation was compared to observations to check the assumptions and parameters within the model (table 4). The results were adequate and comparable, and the model was considered satisfactory and was used unchanged thereafter except for selection of different boundary conditions. Model sensitivity was also carried out to test the model's response to selection of initial and boundary conditions. All sensitivity reported change of less than 5 percent in general for wave heights and wave periods. For instance, a change in water level of 1 m as the initial condition resulted in a change of approximately 2.95 percent on the wave heights and approximately 2.8 percent on the wave periods. For each storm wave, incoming or approaching angles were selected at 45, 90, 135, 180, and 235 degrees. In addition, a cold front or winter storm was simulated with northwesterly winds, which are typical after the passage of a front.

Wave Propagation

The wave boundary condition is located in deep water (much greater than 200 m). The propagation of wave energy directly off the boundary inwards is not affected by any finite water effects, as can be seen from the nearly constant wave period (fig. 6). The wave direction is identical to the wind direction, and hence the wave period remains more or less constant over the initial several kilometers. At the east side boundary, the effect of the decreasing depth can be seen in the upper part of the grid (fig. 6). The wave height decreases significantly when the waves propagate over the coastal shelf break, which can be observed in the region indicated by the solid ellipse in figure 6*A* and also visible in 6*B*. Refraction of incoming wave rays can also clearly be seen in these results for the largest grid by the changing vector directions, which indicates that already at deeper waters (greater than 50 m), waves can "feel" the presence of the bottom topography.

Wave heights and periods are higher at the northern part of the Chandeleur Islands, where a large tidal inlet stretches to the north of the barrier islands (fig. 6*A*). The northern part of the barrier islands is clearly more exposed to higher wave energy than is the southern part because the deeper isobaths penetrate closer to the barrier islands. As a result, larger wave energy propagates closer to the barrier islands

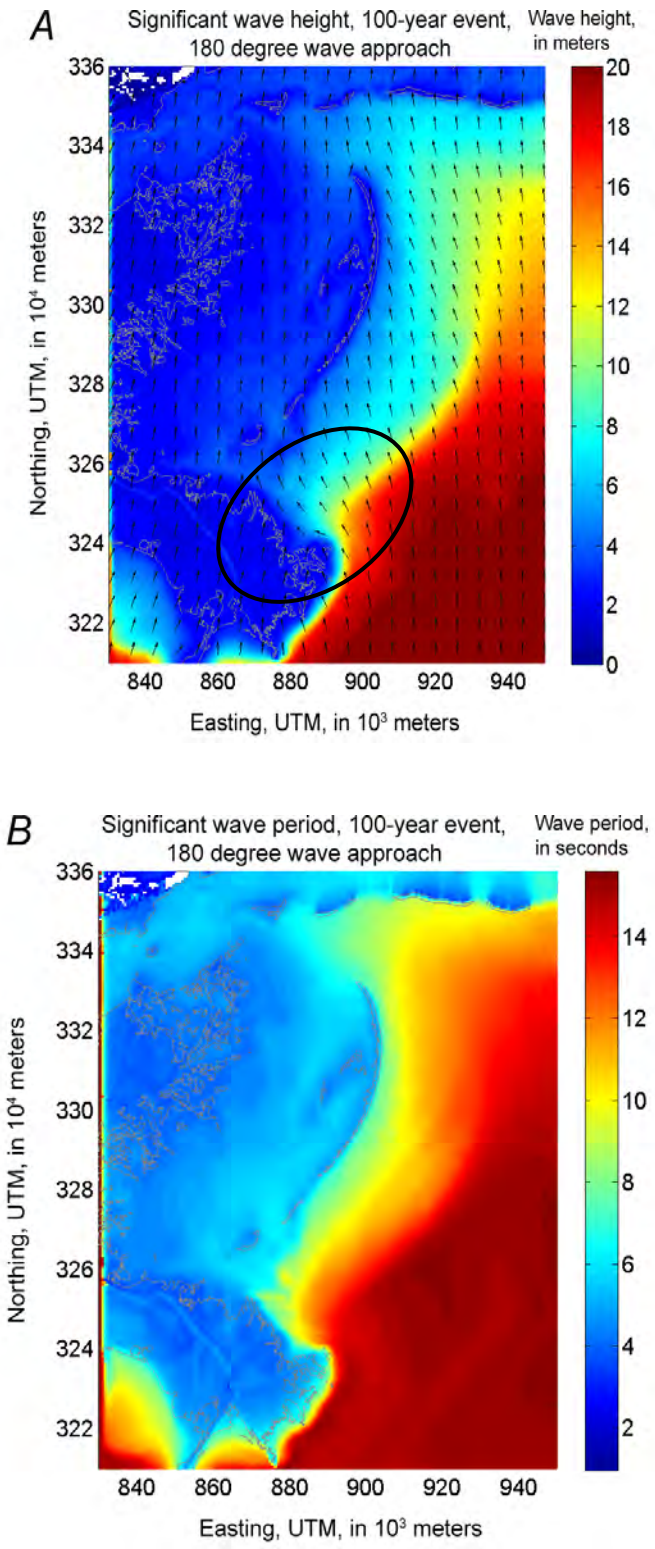

Figure 6. *A*, Wave height H_{m0} and *B*, wave period $T_{m-1,0}$ of results of grid "GridLarge" for a return period of 100-year and an incoming direction of 180 degrees predicted by using the numerical model Simulating WAves Nearshore (SWAN).

before undergoing transformation and dissipation. It is also noted here that the local wave direction in the southern part is relatively more perpendicular to the depth contour lines or isobaths than in the northern part.

Bottom Velocity

From the boundary inwards (from the southeast corner), bottom velocities are zero, indicating that conditions are truly deep water (fig. 7). Propagating nearshore, an increase of the U_{bot} can be observed at the first break of the shelf, indicated with the dashed ellipse (fig. 7). As depth decreases, the presence of the bottom is felt by incoming waves, and the bottom velocity increases as a result. The bottom excursion velocities soon become significant, up to 1 m/s. The excursions in bottom velocity persist up to the second shelf break (see the solid ellipse in fig. 7). Here, orbital velocities become large, and surf breaking occurs. Wave energy is further dissipated over the shallow foreshore, shoreface, and near the Chandeleur Islands where orbital velocities in excess of 1 m/s are still observed. Further to the north, at the large tidal inlet between Hewes Point and the Mississippi barrier islands, bottom velocities are larger than at the central part and southern end of the barrier island chain.

Dissipation Terms

In deeper water, the whitecapping term is dominant (fig. 8*A*), which can be explained by the fact that in the energy balance equation, wind input at deep water results in an increase of wave steepness. Part of the energy is then redistributed over frequencies, but most of it is dissipated by whitecapping. In shallower waters, the presence of the bathymetry results in wave shoaling with steeper waves as well. Breaking of these waves is accounted for by the surf dissipation term. There is clearly dissipation over the bars in front of the barrier islands (fig. 8*A*, left, and 8*B*, left), as well as the confined surf zone near the beach line of the barrier islands.

For the 1-year return period, the energy transfer from wind into the wave field is much lower, and hence all action balance terms are lower in absolute sense (fig. 8*C*). The presence of the shelf break is not observed anymore in the surf dissipation term. At deeper waters, whitecapping continues to be the predominant process, which indicates that for smaller return periods, the active surf zone is much more confined. Since depth-limited breaking occurs in the nearshore for both storm waves, the nearshore dissipation is similar, except for differences in breaking that are produced by the storm surge associated with each storm wave. Larger storms in this study were assumed to be accompanied by higher storm surge, therefore producing small differences in the size of the surf zone.

Implications for Sediment Transport

After analyzing all of the SWAN simulations (comparing the breaking wave angle relative to the shoreline), it was concluded that for incident wind and wave directions of 90 degrees (azimuth), the resulting longshore current indicates a nodal point in the central portion of the Chandeleurs. South of this point, the longshore current is directed southwards, and north of this point, longshore currents are directed northwards. This observation confirms results presented by the one-dimensional model and is consistent with the literature (Georgiou and others, 2005; Ellis and Stone, 2006). With increasing incoming wave and wind direction from the south, the longshore current along the barrier islands is directed northward along the entire barrier island chain. Therefore, for all simulations performed herein, and for incoming wave directions of greater than about 110 degrees and large incident wave heights and periods, longshore currents are mainly directed north. A northward transport direction is even more apparent during storms, especially those that pass westward of the barrier islands because they produce wind directions that range from 90 degrees to 180 degrees. Such observations further emphasize the importance of these storms not only on the evolution of the barrier island chain but also on the redistribution of the sand to the north.

Bottom Velocity

In addition to surf zone processes and longshore sediment transport resulting from storm waves and fair weather conditions, sea floor change analysis performed by Miner and others (this volume) indicate large erosion of the lower shoreface at depths that are beyond the fair weather wave base. Eroded and accreted sediment volume measured in this study cannot be accounted for by typical sediment transport in the littoral zone. These areas are active, however, during large or even intermediate storms (fig. 9) and may become part of the littoral transport system. We point out here that the shelf break plays a critical role in controlling large wave dissipation by reducing wave velocities by approximately 2 m/s. This dissipation is almost irrespective of incoming wave direction. For lower return periods, the extent of the area with large bottom velocities is far less but is substantial nonetheless. For instance, return periods of 10 years produce bottom velocities of 1.5 m/s at depths of approximately 50 m, and 1-year return period storms produce velocities of approximately 1 m/s at similar depth. These results indicate that the entire lower shoreface is active at least once a year for transport and that at least once every 10 years substantial erosion can be expected.

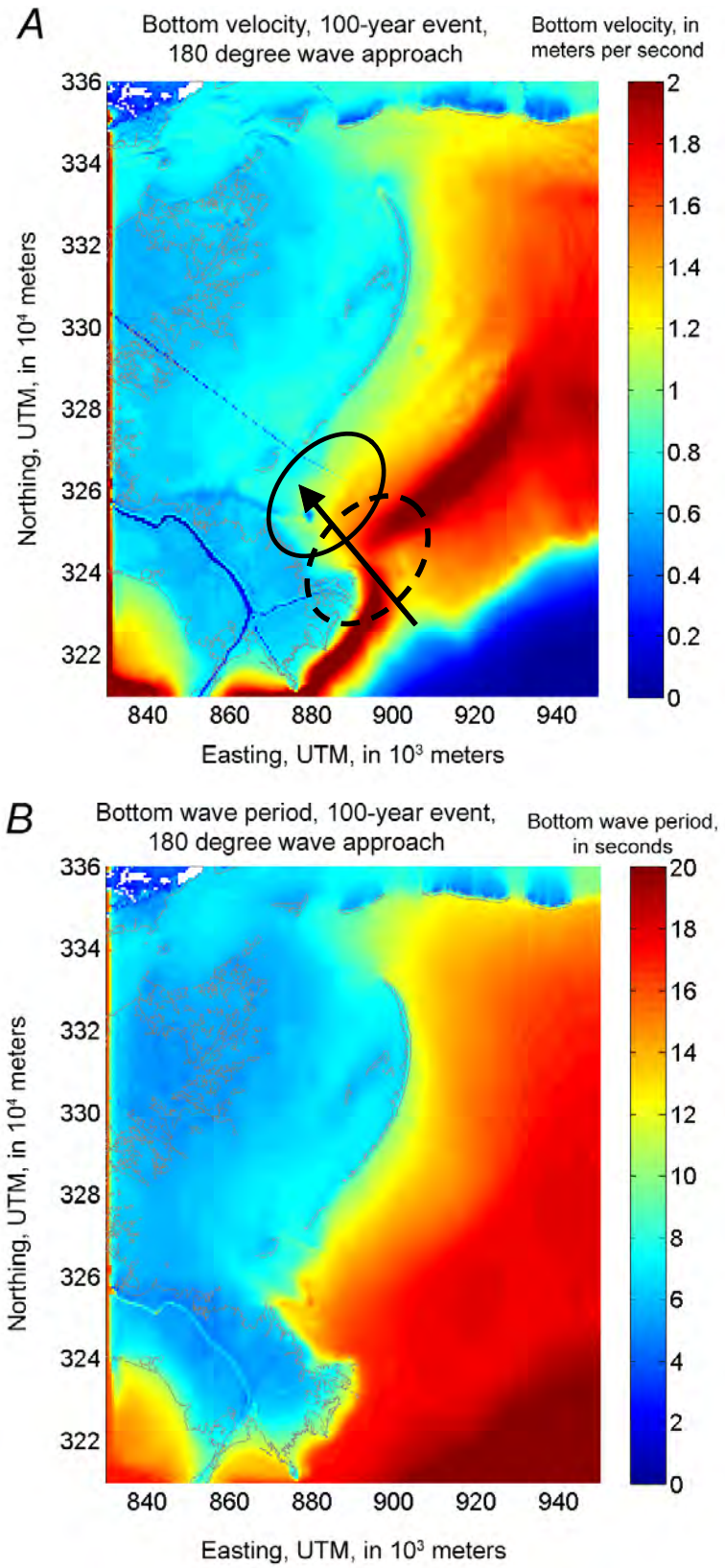

Figure 7. *A*, Bottom velocity U_{bot}. *B*, Bottom wave period T_{mBot}.

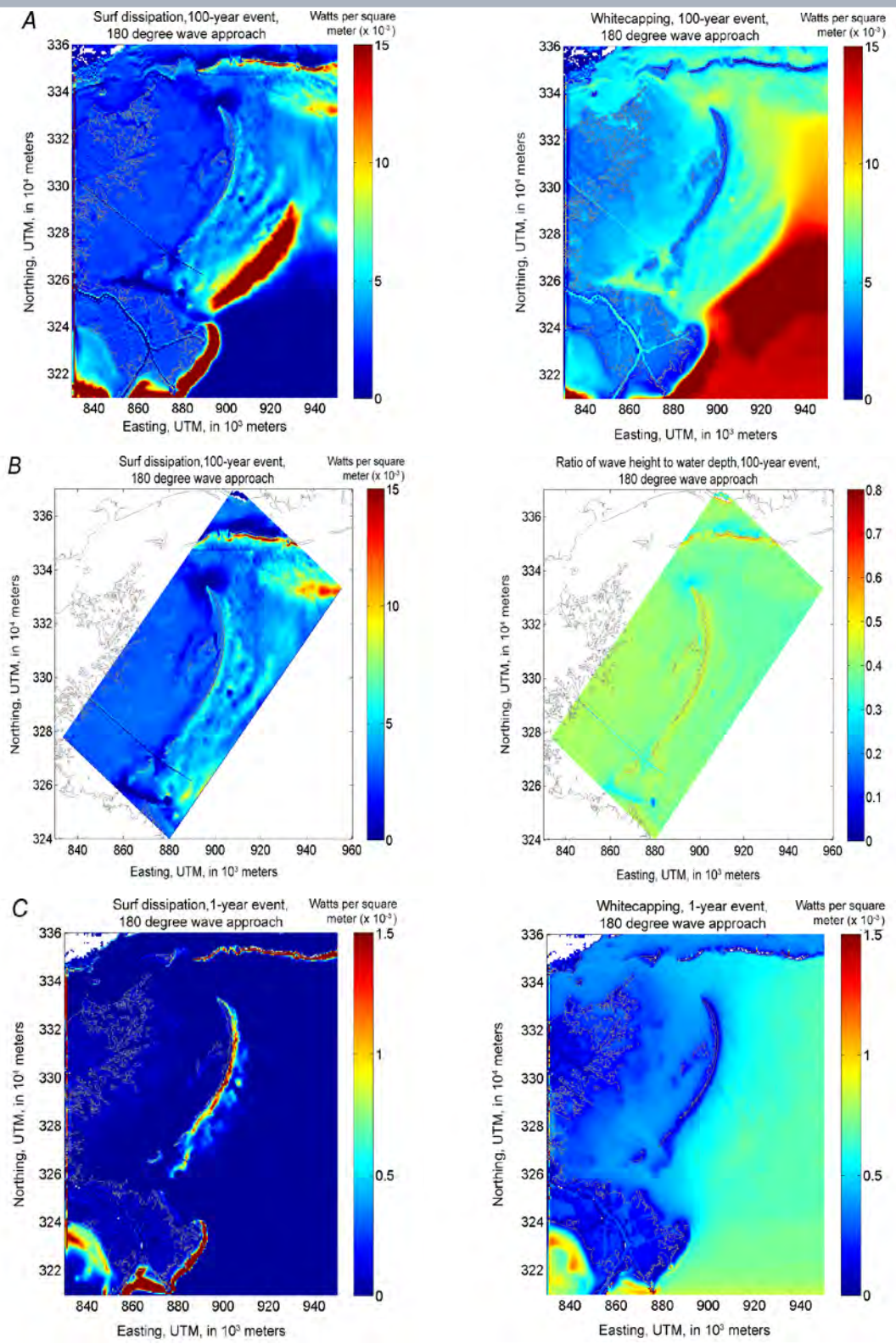

Figure 8. *A*, Surf breaking dissipation (left panel) and whitecapping (right panel) plotted at the same scale for 100-year event and 180 degrees. *B*, Surf dissipation and $H_{m0/d}$ ratio of the nested grid for 100-year event and 180 degrees. *C*, Surf breaking dissipation and whitecapping for 1-year event and 180 degrees.

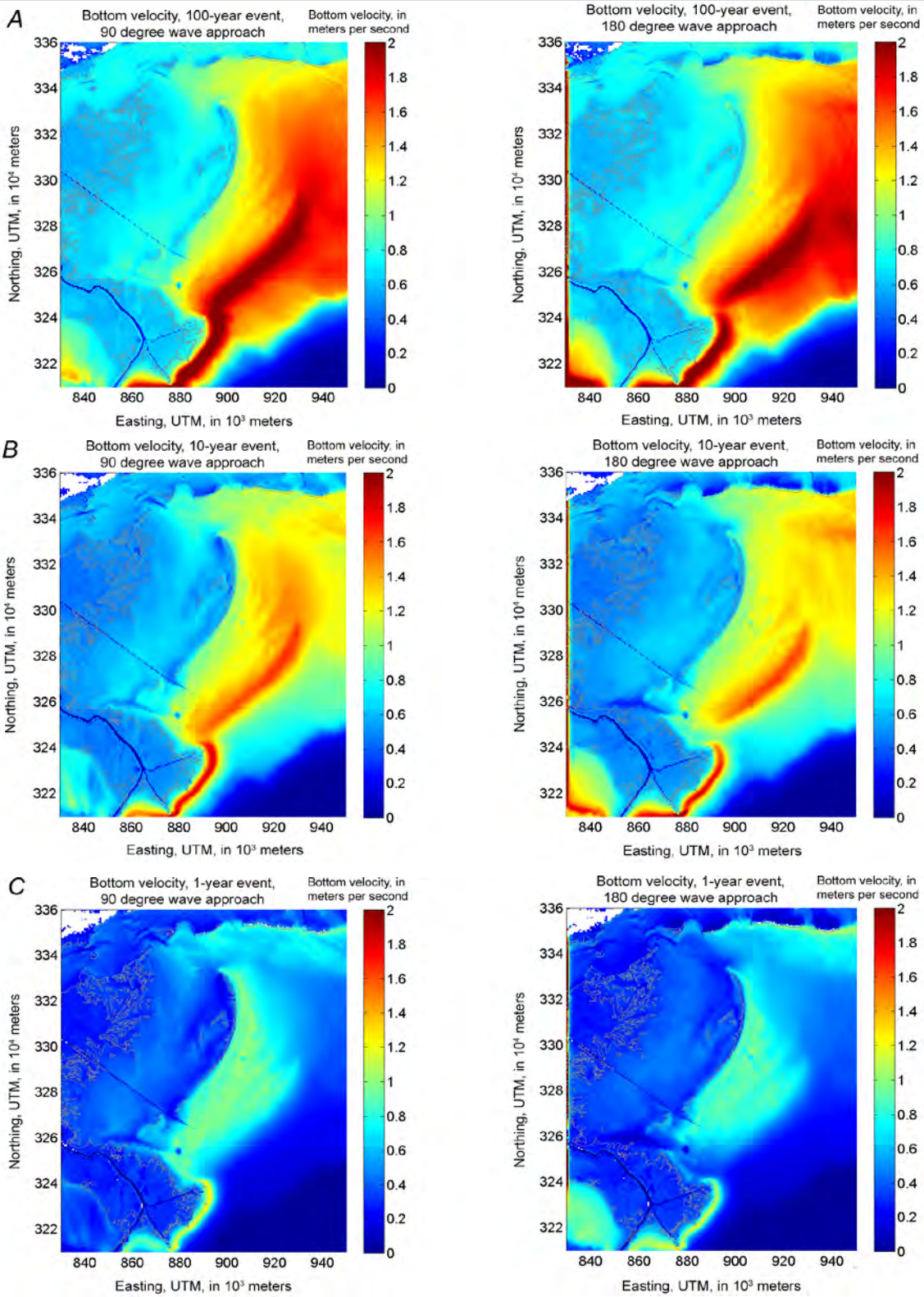

Figure 9. Bottom velocity for incoming waves of 90 and 180 degrees for the 100-year, 10-year, and 1-year return period storms. *A*, 100-yr event and 90 degrees (left panel) and 180 degrees (right panel). *B*, 10-yr event and 90 degrees (left panel) and 180 degrees (right panel). *C*, 1-yr event and 90 degrees (left panel) and 180 degrees (right panel).

Winter Storms and Cold Fronts

Northwest of the Chandeleur Islands, finite water wave growth is observed around the Biloxi Marshes with a wave height up to 1 m and a wave period of 3 seconds. At the northern tip of the Chandeleurs, near Hewes Point, wave height increases further because of increasing depth (fig. 10*A*). The same observations appear for the wave period, which increases to values over 4 seconds (fig. 10*B*). At this point waves also refract in the southward direction because of increasing depth.

Orbital velocities near the sea floor do not exceed values of 0.4 m/s (fig. 11*A*), which is much less than the values simulated during larger storms and hurricanes, where values were in excess of 2 m/s. This difference can mainly be attributed to the fact that a growth limit exists for waves growing over shallow waters, and hence both wave height and wave period are limited by depth. As a result of depth-limited waves, bottom velocities are rather small and cannot grow beyond these limitations. While the same limitations exist for larger storms, these storms are typically associated with higher storm surge, which allows for additional wave growth. Surf dissipation is only observed in areas with depth gradients, and the largest dissipation is observed at the northern tip of the Chandeleur Islands. In this area, incoming waves from the northwest refract and dissipate their energy around the Hewes Point spit, reshaping it in both directions. This energy is also important in reworking the sand that may exist landward of the backbarrier.

Tide-Induced Currents

Tide-induced currents in the vicinity of the Chandeleur Islands and the Chandeleur and Breton Sounds are perhaps not strong enough to mobilize sand because of the microtidal regime, but these currents can be very effective in transporting finer material once in suspension. To study the distribution and magnitude of tide-induced currents in the study area, a numerical model was used. The finite volume coastal ocean model (FVCOM; originally developed by Chen and others, 2003) has successfully been applied to southeast Louisiana by Georgiou and others (2007) and by McCorquodale and others (2008). In this study, the model spinup time was 2 days, and the remaining 28 days included two spring/neap cycles (fig. 12). In tidal inlets and small curved channels, the model predicted residual velocity patterns similar to those observed by Li and others (2008). In the vicinity of tidal inlets, depth-averaged velocities exceeded 1.0 m/s during the spring tides, while residual currents averaged through the entire simulation appeared to be 0.25 m/s, and they were generally higher in the north end of the barrier island chain compared to the central portion.

While residual currents provide insight into the available energy in the water column to transport fine material, they also provide potential preferential pathways for flow through the barrier island chain, and perhaps information on available pathways for storm-induced flow. Tidal inlets undergo approximately 1 m/s higher velocities than do other shorelines (fig. 13) and can be used to infer potential transport of sediment through these inlets given material in suspension from an event (that is, a cold front). Once in suspension, these currents can also be used to infer the potential of this material to be imported into the bays and sounds or to be exported offshore.

Storm-Induced Circulation and Transport

During storms, waves activate deeper areas offshore and subject the bed to applied shear stresses suitable for erosion. This erosion was observed in the sea floor change analysis by Miner and others (this volume) and was reported by List and others (1997) and Jaffe and others (1997) for studies west of the modern delta of the central Louisiana coast. Once this material is eroded, and while in suspension, it can leave the system by means of circulation during the event. Circulation patterns during a storm can maintain particles in suspension and given enough turbulence in the water column can transport them outside the system—offshore or onshore. Conditions may be such that (1) this material never returns to the vicinity of the barrier islands or (2) the return takes place over a longer timescale or with a different process or mechanism. To investigate and quantify this process are extremely difficult without observations of the specific event. There are several unknown parameters that not only are not available in literature but also have time-dependent properties that make it impossible to capture both spatially and temporally. For instance, we know very little about the strength, cohesion, erosion rates, and in situ properties of prodelta material, which is the material that underlies the St. Bernard Delta Complex. In addition, bottom boundary layer development during a storm and accurate measurements of currents near the bed are also largely unknown except in much deeper water from acoustic current profilers. For this purpose, numerical tools can help provide a first-order estimate and give enough information to direct further studies and measurements. To achieve this, the Advanced Circulation Model (ADCIRC) was used with post-Katrina bathymetry (Resio and Westerink, 2008). This coupled wave-storm surge model was used to perform a suite of simulations for lower intensity storms (Sleath and others, 2009) rather than extremely large events because the lower intensity events have smaller return periods. A suite of hypothetical storms were used, which were developed by the U.S. Army Corps of Engineers (2006) during post-Hurricane Katrina design and probability analysis. Several storms were simulated with tracks passing both east and west of the barrier islands within approximately 40 km. A direct hit on the Chandeleur Islands was not investigated. For simplicity, shore-perpendicular

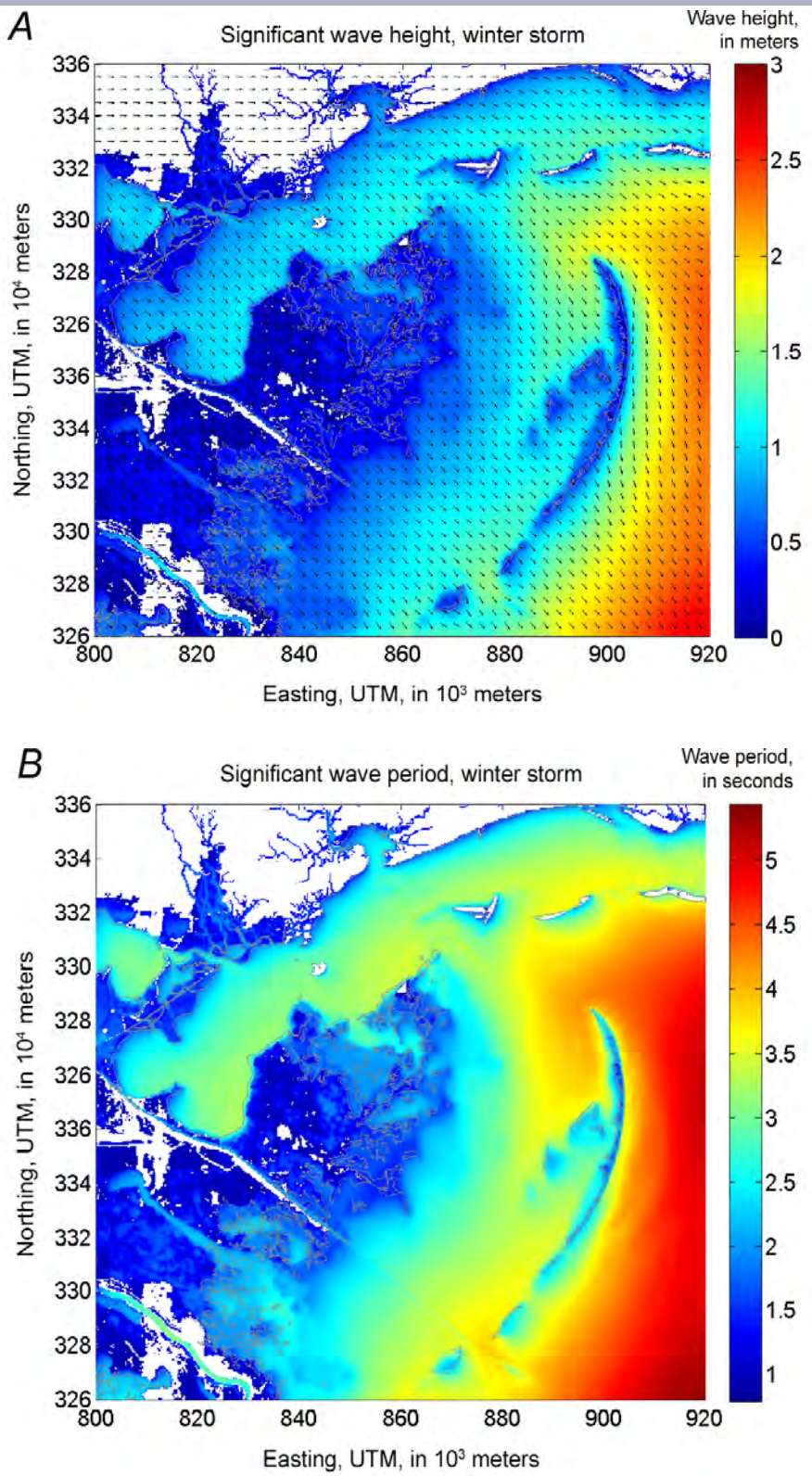

Figure 10. *A*, Wave height H_{m0} of the winter storm. *B*, Wave period $T_{m-1,0}$ of the winter storm.

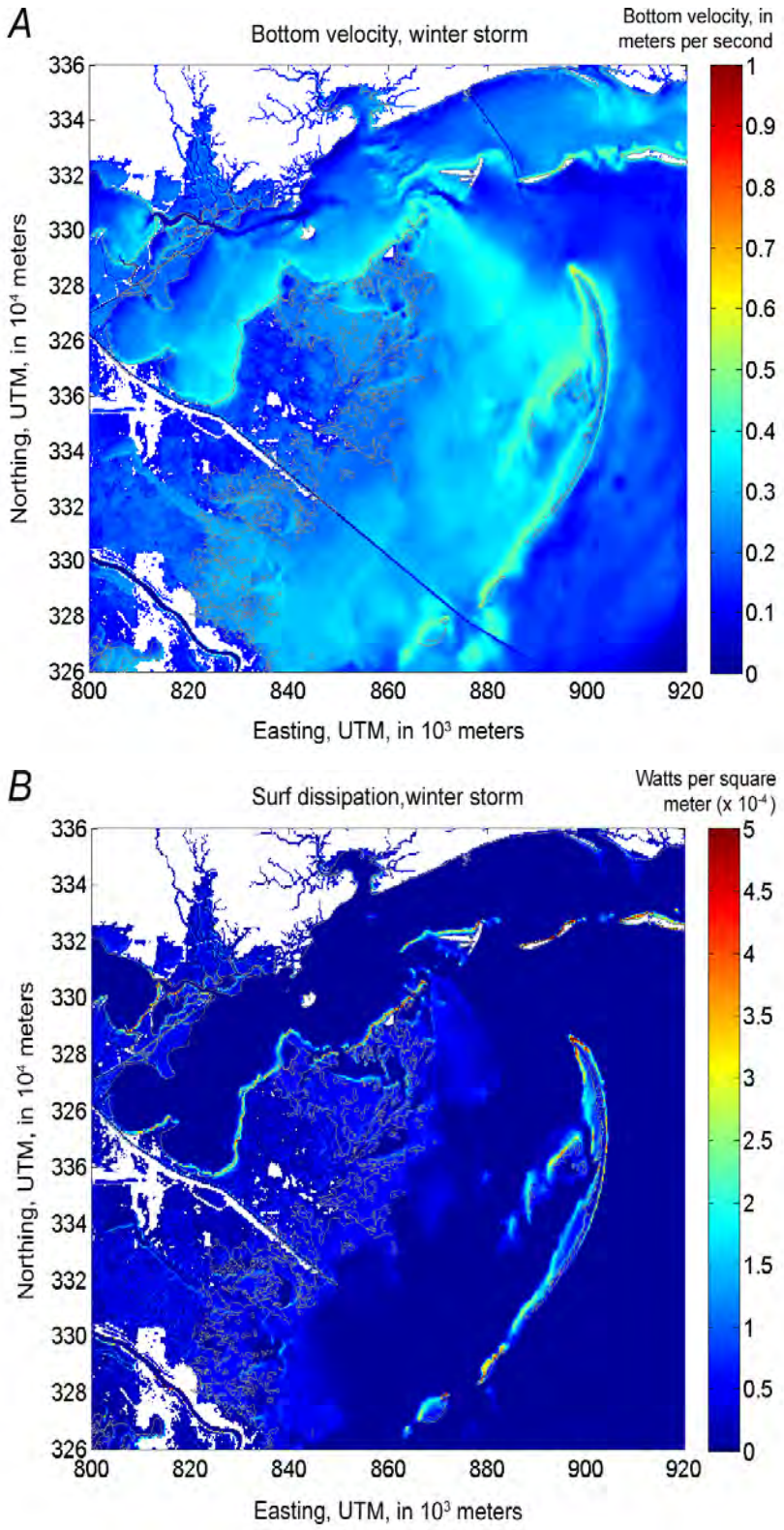

Figure 11. *A*, Bottom velocity U_{bot} during a winter storm simulation. *B*, Surf dissipation in a winter storm simulation.

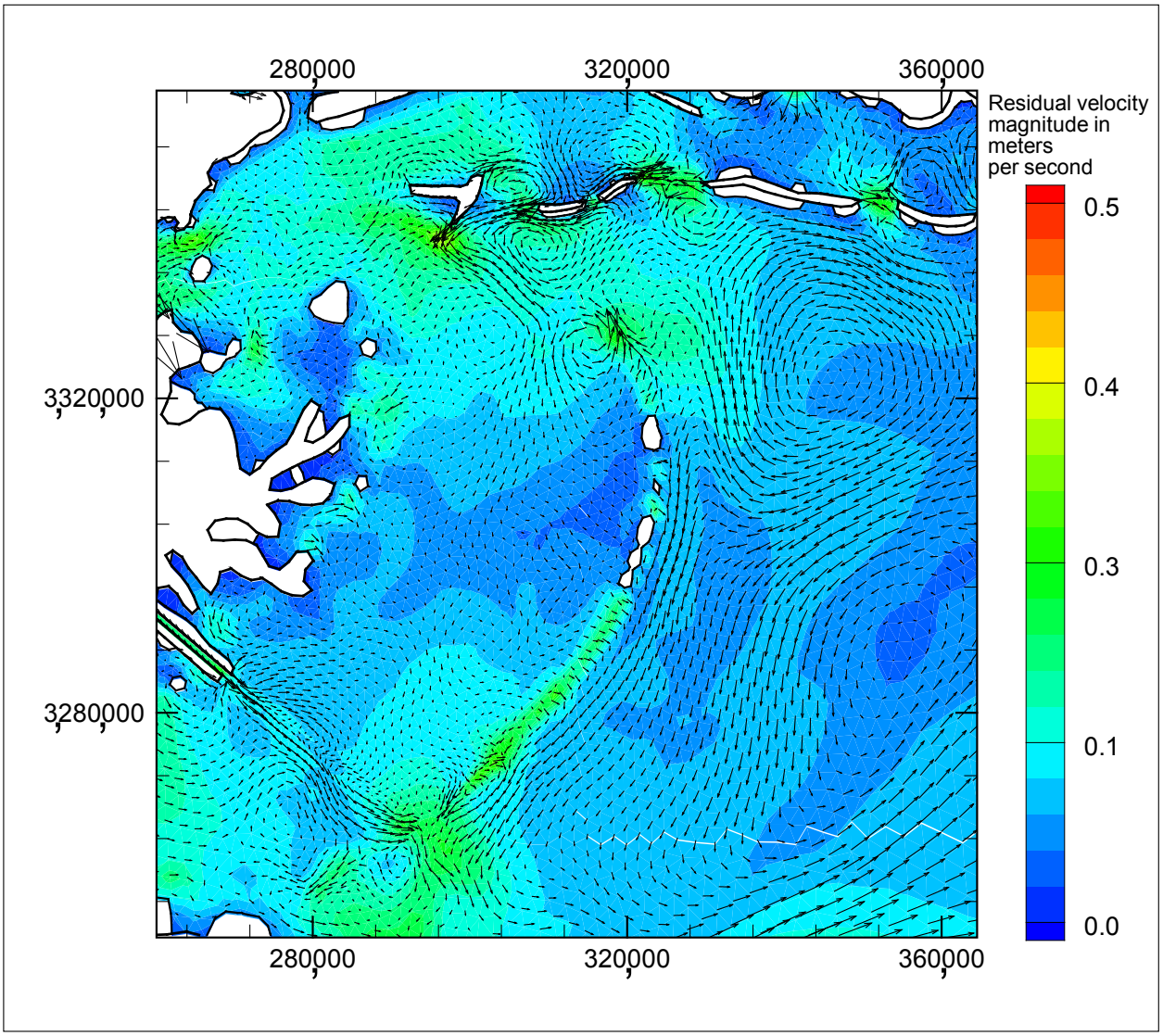

Figure 12. Residual tidal currents (depth-averaged) after a 30-day tidal simulation without wind forcing. Velocity vectors indicate direction, while the color contours indicate magnitude.

profiles were selected to extract velocity and water surface elevation (surge) information. The model output time-dependent information every 30 minutes along this profile, which extended beyond the lower shoreface into water depths beyond 30 m. Information and discussion that follow are based on one of these profiles (fig. 14). The history, during the development of the storm, is shown along this profile (fig. 14) to characterize general circulation in the vicinity of the barrier islands during such events and infer resulting transport.

Of particular importance in the storm surge simulations was the overtopping of the barrier islands with a rather small intensity storm (fig. 15), which was primarily due to the fact that the elevation post-Katrina generally showed low subareal exposure and very little dune fields. Ground observations also reported the highest dunes 2 years after Hurricane Katrina in the north-central portion of the Chandeleur Islands to be approximately 1.2–1.4 m in height. We note that this elevation will most likely be exceeded during an intermediate event or a low-intensity storm. The values shown in figure 15 (an averaged storm surge of approximately 0.5 m in the vicinity of the barrier islands as the storm nears and a maximum surge of 1.2 m) do not include the wave setup, which would only increase the maximum surge observed near the islands. At time 96 hours, the barrier islands are overtopped, and overland

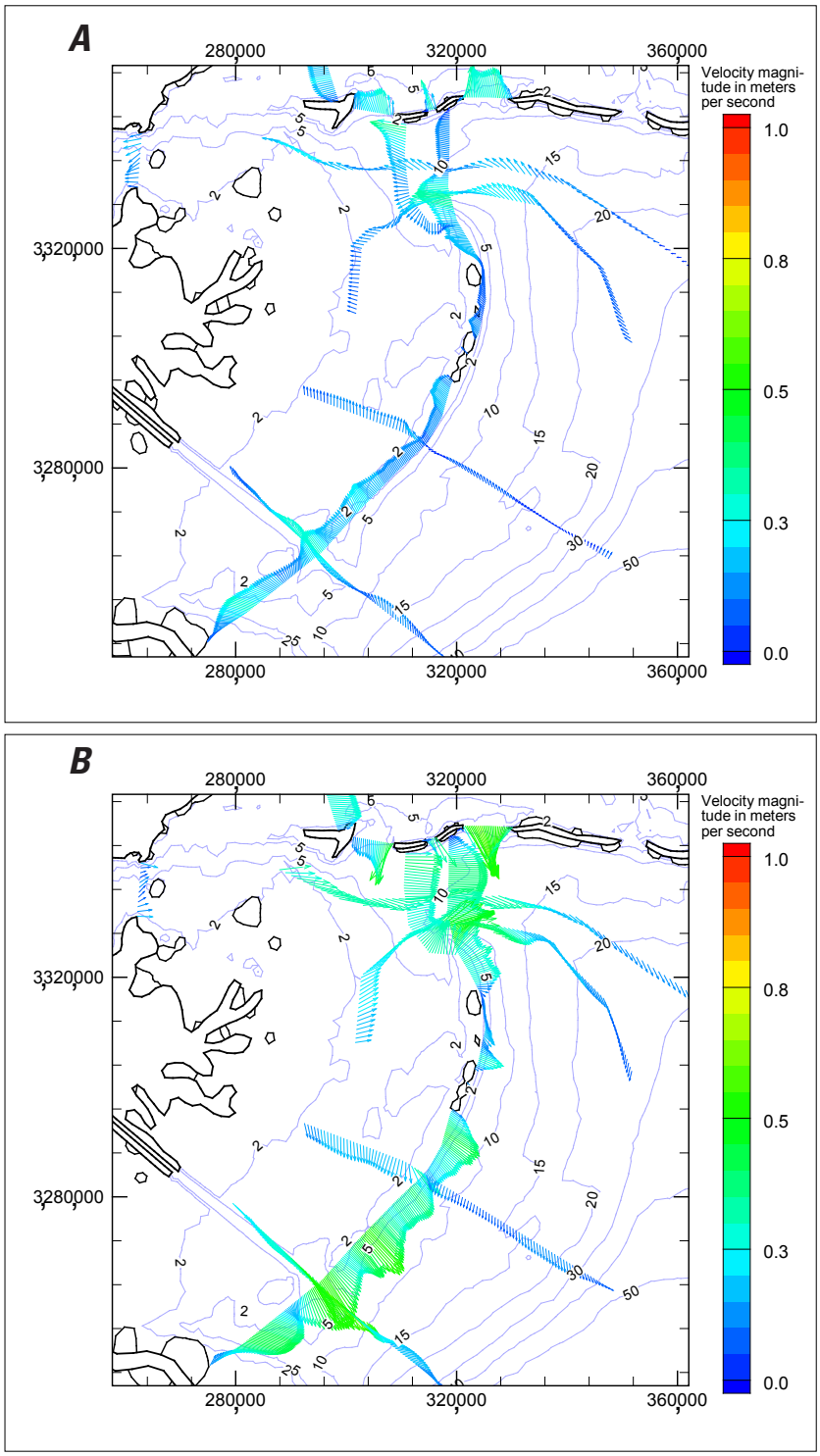

Figure 13. *A*, Maximum tidal current magnitude (colored) and direction (vector) for spring tides during flood. *B*, Maximum tidal current magnitude (colored) and direction (vector) for spring tides during ebb. Note the broad sheet of high-velocity areas in the ephemeral sand bodies (previously known as Curlew and Grand Gosier Islands) and through other inlets across the barrier islands including the one north of Hewes Point between the Chandeleurs and the Mississippi barrier islands.

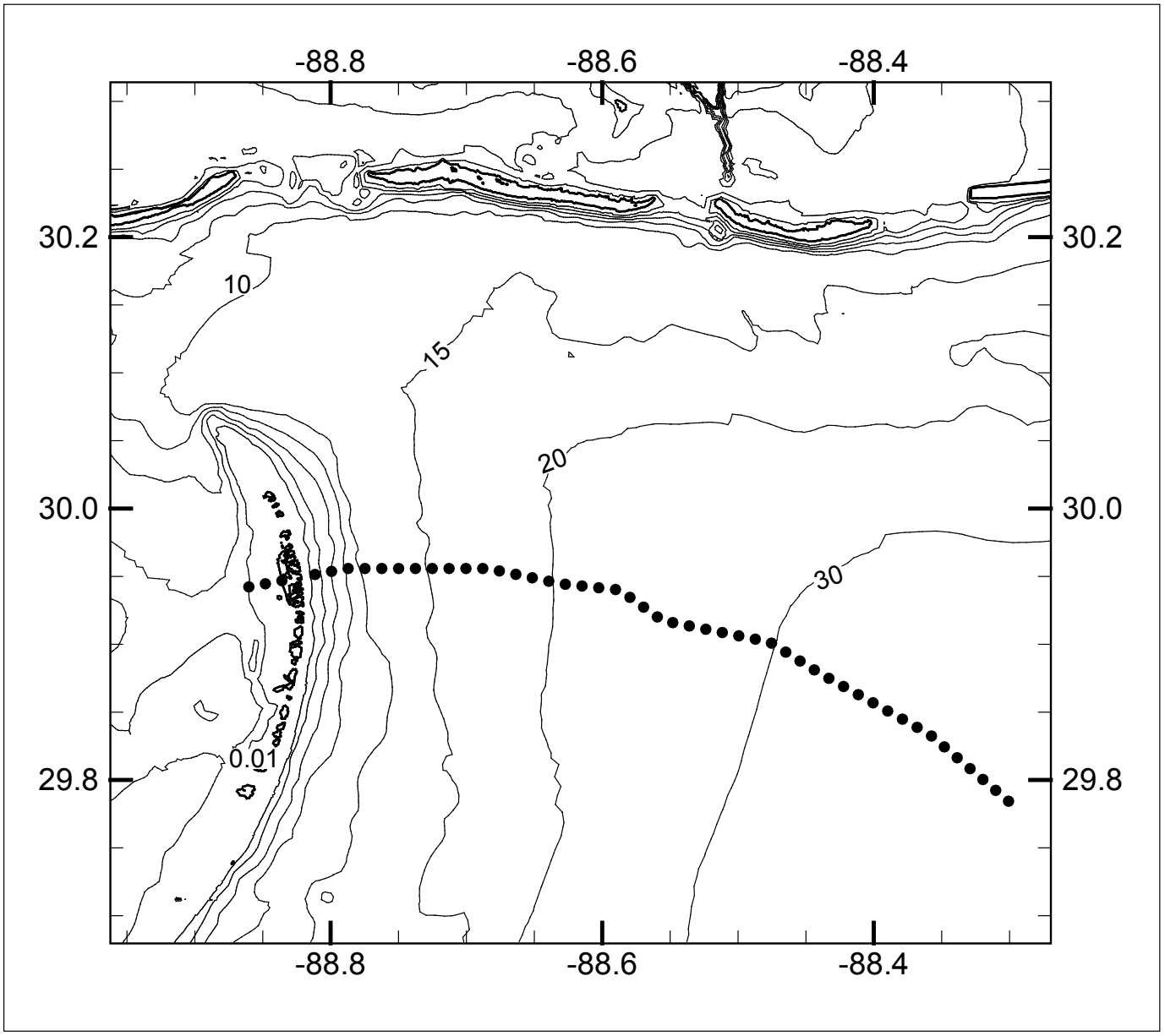

Figure 14. Shore-perpendicular profile showing the data extraction during the Advanced Circulation (ADCIRC) storm simulations (Sleath and Georgiou, 2009).

flow occurs for the majority of the barrier islands (fig. 15). Velocities of 1 m/s are observed, directed westward, as flow is directed over the barrier islands. At this instant, velocities of up to 0.5 m/s are also observed at offshore depths of 12–15 m (indicated in the upper panel of fig. 15 by the gray box). As the storm moves farther north and wind fields change, water and surge start to recede and are directed eastward. Setup in the backbarrier forces water over the barrier islands again (shown in fig. 15 to be directed eastward) with magnitudes of 0.5–0.6 m/s. Shortly after, northwesterly winds and the relaxation scale of the event drive water to move toward the southeast with velocities of 0.5 m/s. This velocity is similar to offshore depths of approximately 20 m. When the surge recedes more, the barrier islands are no longer overtopped, and conditions slowly relax and return back to normal tidal conditions. It should be noted that the velocity and elevation shown in figure 15, in particular when the barrier island is inundated, may show higher than expected pressure gradients across

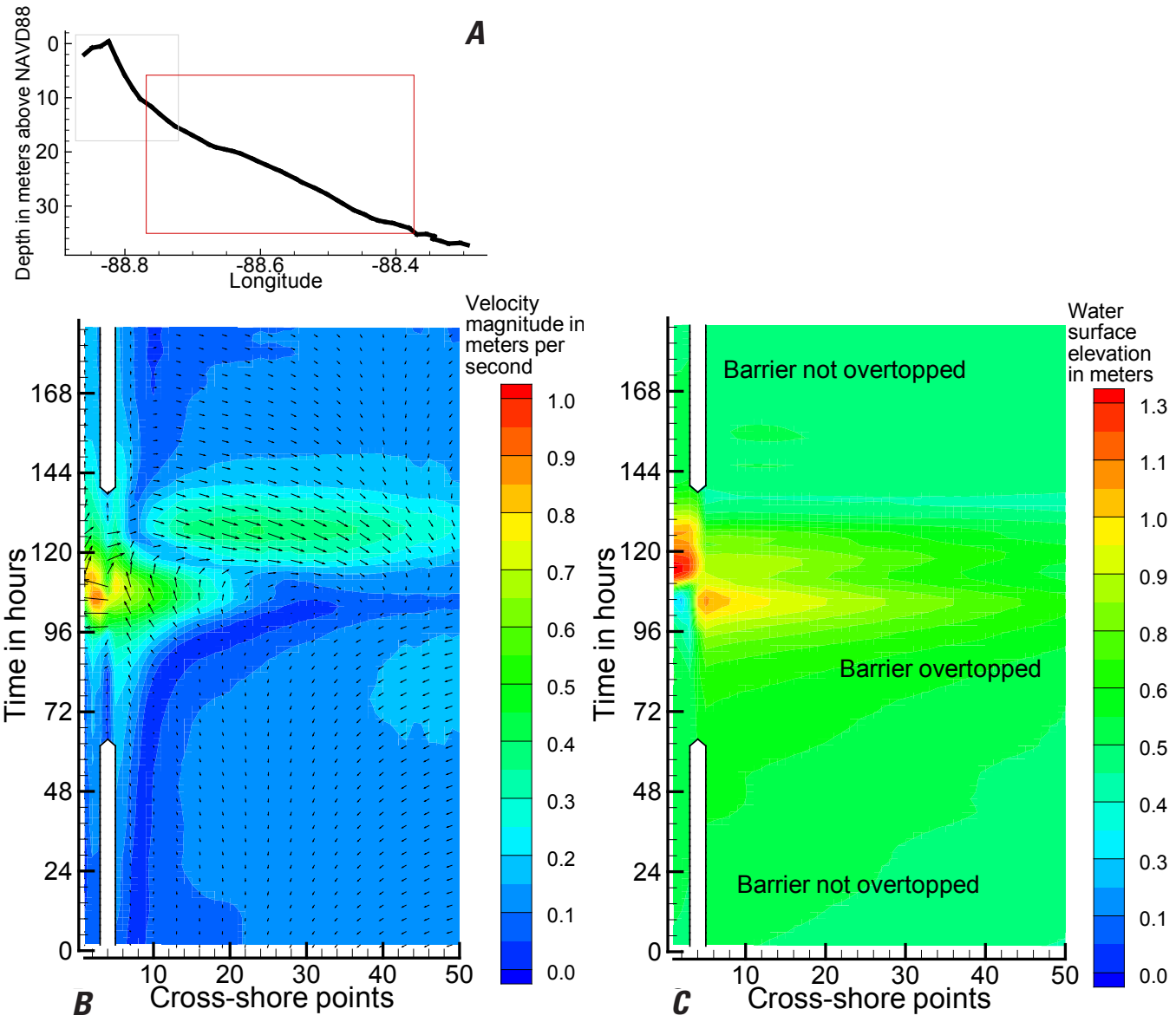

Figure 15. Evolution of the depth-averaged velocity magnitude (color), direction (vector), and storm surge during a storm along the profile shown in figure 14. Information starts at about 1 day before the storm is felt in the area. Therefore, time zero corresponds to approximately 1 day prior to the storm being in the vicinity of the modern delta. The specific storm in this figure has a track that is west of the Chandeleur Islands going northward over the east edge of the Biloxi Marshes and a central pressure of 975 millibars, 11 kn forward speed, and 11 nmi radius to maximum winds. *A*, Cross-shore depth. Gray box shows the active barrier bed during the advancement of the storm, and red box shows the active bed during the return flow. The y-axis indicates the depth at which derived data are displayed. *B*, Time-dependent velocity (cross-shore points refer to the individual points shown in fig. 14). *C*, Storm surge (cross-shore points refer to the individual points shown in fig. 14). NAVD 88, North American Vertical Datum of 1988.

the barrier islands, and as a result a higher velocity could be observed. These high pressure gradients are not necessarily true, even with extreme setdown in the backbarrier, and may be an artifact of the extracted information from the model nodes. The general circulation pattern and the time-dependent evolution of the profile (as well as the relative physical processes) are, however, captured accurately and provide insight into the evolution of water surface elevation and velocities along the barrier islands.

Discussion and Conclusions

The Chandeleur Islands are undergoing rapid transgression or transgressive submergence (Miner and others, this volume). The barrier islands have been impacted severely by storms in the last decade, and there has been a very slow process of recovery. A similar recovery of this system after Hurricanes Camille (1969) and Betsy (1965) was possible because of the subsequent quiescent period of 25 years, during which no named storms were recorded until Hurricane Andrew in 1992. During this quiescent period, the Chandeleur Islands built a substantial subaerial footprint, large enough to absorb substantial energy from Hurricane Georges in 1998. Some recovery after Hurricane Georges gave the barrier islands sufficient footprint to withstand the immense forces of Hurricane Ivan (2004); however, a year later and with little defense, the barrier islands were completely obliterated by Hurricane Katrina. The entire sand volume in the system disappeared and was only seen in the form of offshore bars that slowly started to migrate onshore after several months. With sand not seen in the immediate footprint of the barrier islands for months post-Katrina, the Chandeleur Islands' recovery period slowly started (as recorded in this volume). Not long after, Hurricanes Gustav and Ike (2008) caused additional impacts on the Chandeleur Islands that were of different nature and scale. Field observations of subsurface methods (Twichell and others, this volume), coring and grain-size analysis (Flocks and others, this volume), and shoreline change analysis (Fearnley and others, this volume) suggest that the north portion of the barrier island is not migrating or eroding as fast as is the southern portion, that there exists sufficient sand in the system, and that some progradation has been observed. The central and southern portions of this barrier island chain are undergoing extreme change with rapid erosion rates that are perhaps due to coastal straightening response to modern delta progradation. The longshore sediment transport rates produced herein and those that exist in the literature cannot explain the volumes of sand identified by other studies in this report. These processes, however, have been operating in a similar way since the last abandonment of the St. Bernard Delta Complex. We note that during storms with return periods of 1, 10, and 100 years, wave modeling has shown that northward transport is dominant. This dominance in fact occurs when incident wave angles are greater than 110 degrees. A storm with a typical path to the west of the barrier islands will produce winds and wave conditions that will have incident angles in excess of 90 degrees for more than 75 percent of the time. In addition, during these events, rates of transport can more than double because transport rates predicted by the CERC equation (Coastal Engineering Research Center, 1977) are proportional to the wave height raised to the 5/2 power or $H^{5/2}$. Since fair weather wind and wave energy is not available to rework this material and redistribute it back in the littoral system, large accumulation rates take place on the northern portion of the barrier island and especially close to Hewes Point. In addition, the large accommodation space that exists north of the Hewes Point spit acts as a sink of sediment that is permanently lost from the littoral system. Winter storm simulations performed herein have demonstrated some ability to rework some of this sediment back into the littoral system; however, these waves are not large enough because of an imposed depth-limited condition, and large volumes of sand are beyond the wave base. It is therefore difficult for this sediment volume to return to the littoral system and subsequently rework toward the central and southern portion of the barrier islands. Storm wave simulations have also indicated that large areas of the lower shoreface are activated during storms and undergo erosional conditions for several hours during one storm event. Circulation patterns from storms have also indicated that there is sufficient turbulence in the water column to erode and transport material outside the littoral system in areas where it cannot be returned with normal fair weather processes. In summary,

- The Chandeleur Islands are undergoing high rates of transport in the northward direction during high-intensity and intermediate storms.
- Large areas of the lower shoreface are activated and are undergoing erosion during intermediate and large storms.
- There is little or no fair weather mechanism to rework material into the littoral system.
- There is a net sediment loss from the system.

References

Chen, C., Liu, H., and Beardsley, R., 2003, An unstructured grid, finite-volume, three-dimensional, primitive equations ocean model—application to coastal ocean and estuaries: Journal of Atmospheric and Oceanic Technology, America Meteorological Society, v. 20, p. 159–186.

Coastal Engineering Research Center, 1977, Shore protection manual: Washington, D.C., U.S. Army Corps of Engineers, Coastal Engineering Research Center.

Ellis, J., and Stone, W.G., 2006, Numerical simulation of net longshore transport and granulometry of surficial sediments along the Chandeleur Island, Louisiana, USA: Marine Geology, v. 232, p. 115–129.

Georgiou, I.Y., Fitzgerald, D.M., and Stone, G.W., 2005, The impact of physical processes along the Louisiana coast: Journal of Coastal Research, Special Issue 44, p. 72–89.

Georgiou, I.Y., McCorquodale, J.A., Retana, A.G., FitzGerald, D.M., and Hughes, Z., 2007, Hydrodynamic and salinity modeling in the Pontchartrain basin—assessment of freshwater diversion at Violet with MRGO modifications: University of New Orleans, Final Report to the National Oceanic and Atmospheric Administration, 35 p.

Holthuijsen, L.H., Booij, N., and Ris, R.C., 1994, A spectral wave model for the coastal zone, *in* Wiegel, R.L., Magoon, O.T., and Hemsley, J.M., Ocean Wave Measurement and Analysis—Proceedings of the Second International Symposium, Honoring Professor Robert L. Wiegel, New Orleans, Louisiana, July 25–28, 1993: New York, American Society of Civil Engineers, p. 630–641.

Hubertz, J.H., Abel, C.E., Jensen, R.E., Vincent, C.L., 1989, Gulf of Mexico hindcast wave information. Waterways Experiment Station Report, vol. 18: Vicksburg, Miss., U.S. Army Corps of Engineers.

Jaffe, B.E., List, J.H., and Sallenger, A.H., Jr., 1997, Massive sediment bypassing on the lower shoreface of a wide tidal inlet—Cat Island Pass, Louisiana: Marine Geology, v. 136, p. 131–149.

Komar, P.D., 1998, Beach processes and sedimentation (2d ed.): New York, Prentice Hall, 544 p.

Li, C., Chen, C., Guadagnoli, D., Georgiou, I.Y., 2008, Geometry-induced residual eddies in estuaries with curved channels—observations and modeling studies: Journal of Geophysical Research, v. 113, C01005, doi:10.1029/2006JC004031.

List, J.H., Jaffe, B.E., Sallenger, A.H., Jr., and Hansen, M.E., 1997, Bathymetric comparisons adjacent to the Louisiana barrier islands—processes of large-scale change: Journal of Coastal Research, v. 13, no. 3, p. 670–678.

McCorquodale, J.A., Georgiou , I., Retana, A.G., and Roblin, R.J., 2008, Assessment of integrated hydrodynamic and transport for long-term predictions—FVCOM & water quality modeling of the Pontchartrain Estuary including subprovinces 1 and 5, chap. 11a, *in* Twilley, R.R., ed., Coastal Louisiana Ecosystem Assessment & Restoration (CLEAR) Program—a tool to support coastal restoration. v. IV: Baton Rouge, La., Final Report to Department of Natural Resources, Coastal Restoration Division, 491 p. (Available at http://www.clear.lsu.edu/pdfs/clear_report_20081023154426.pdf.)

Penland, S., Boyd, R., and Suter, J.R., 1988, Transgressive depositional systems of the Mississippi Delta Plain—model for barrier shoreline and shelf sand development: Journal of Sedimentary Petrology, v. 58, p. 932 –949.

Peterka, J.A., and Shahid, S., 1998, Design gust wind speeds in the United States: Journal of Structural Engineering, v. 124, no. 2, p. 207–214.

Resio, D.T., and Westerink, J.J., 2008, Hurricanes and the physics of surges: Physics Today, v. 61, no. 9, p. 33–38.

Sleath, A.G., and Georgiou, I.Y., 2009, The impact of barrier islands on low intensity storms in southeast Louisiana: Accepted, American Water Resources Association, Annual Meeting, Abstract, Portland, Oregon, November.

Smith, J.M., 2007, Modeling nearshore waves for Hurricane Katrina. ERDC TNSWWRP-07-6: Vicksburg, Miss., U.S. Army Engineer Research and Development Center. (Available at https://swwrp.usace.army.mil/portal/alias__swwrp/lang__en-US/tabID__3637/DesktopDefault.aspx.)

Smith, J.M., Sherlock, A.R., and Resio, D.T., 2001, STWAVE—steady-state spectral wave model user's manual for STWAVE, version 3.0. ERDC/CHL SR-01-1: Vicksburg, Miss., U.S. Army Engineer Research and Development Center.

Suter, J.R., Penland S.P., Williams, S.J., Kindinger, J.L., 1988, Transgressive evolution of the Chandeleur Islands, Louisiana: Transactions, Gulf Coast Association of Geological Societies, v. 38, p. 315–322.

U.S. Army Corps of Engineers, 2007, Performance evaluation of the New Orleans and southeast Louisiana hurricane protection system: Interagency Performance Evaluation Task Force, Final Report. (Available at https://ipet.wes.army.mil/.)

van der Westhuysen, A.J., Zijlema, M., and Battjes, J.A., 2007, Nonlinear saturation-based whitecapping dissipation in SWAN for deep and shallow water: Coastal Engineering, v. 54, p. 151–170.

Appendix H–1. Wind and Wave Climate Analysis, Wave Recasting, and Simulation of Longshore Sediment Transport (See Index Page To Access Data)

Publishing support provided by
Lafayette Publishing Service Center